2016

Visualizing Herpesvirus Procapsids in Living Cells

Oana Maier
Northwestern University

Patricia J. Sollars
University of Nebraska-Lincoln, patricia.sollars@unl.edu

Gary E. Pickard
University of Nebraska-Lincoln, gpickard2@unl.edu

Gregory A. Smith
Northwestern University

Visualizing Herpesvirus Procapsids in Living Cells

Oana Maier,[a] Patricia J. Sollars,[b] Gary E. Pickard,[b] Gregory A. Smith[a]

Department of Microbiology-Immunology, Northwestern University, Chicago, Illinois, USA[a]; School of Veterinary Medicine and Biomedical Sciences, University of Nebraska—Lincoln, Lincoln, Nebraska, USA[b]

ABSTRACT

A complete understanding of herpesvirus morphogenesis requires studies of capsid assembly dynamics in living cells. Although fluorescent tags fused to the VP26 and pUL25 capsid proteins are available, neither of these components is present on the initial capsid assembly, the procapsid. To make procapsids accessible to live-cell imaging, we made a series of recombinant pseudorabies viruses that encoded green fluorescent protein (GFP) fused in frame to the internal capsid scaffold and maturation protease. One recombinant, a GFP-VP24 fusion, maintained wild-type propagation kinetics *in vitro* and approximated wild-type virulence *in vivo*. The fusion also proved to be well tolerated in herpes simplex virus. Viruses encoding GFP-VP24, along with a traditional capsid reporter fusion (pUL25/mCherry), demonstrated that GFP-VP24 was a reliable capsid marker and revealed that the protein remained capsid associated following entry into cells and upon nuclear docking. These dual-fluorescent viruses made possible the discrimination of procapsids during infection and monitoring of capsid shell maturation kinetics. The results demonstrate the feasibility of imaging herpesvirus procapsids and their morphogenesis in living cells and indicate that the encapsidation machinery does not substantially help coordinate capsid shell maturation.

IMPORTANCE

The family *Herpesviridae* consists of human and veterinary pathogens that cause a wide range of diseases in their respective hosts. These viruses share structurally related icosahedral capsids that encase the double-stranded DNA (dsDNA) viral genome. The dynamics of capsid assembly and maturation have been inaccessible to examination in living cells. This study has overcome this technical hurdle and provides new insights into this fundamental stage of herpesvirus infection.

The herpesvirus structure consists of a double-stranded DNA (dsDNA) genome encased in an icosahedral capsid, which is surrounded by a tegument protein layer and a lipid envelope. Capsid assembly occurs in the nucleus in infected cells, beginning with a spherical procapsid precursor built around a protein scaffold that matures into a DNA-containing angularized capsid (reviewed in reference 1). Subsequently, mature capsids egress from the nucleus to the cytosol, where they acquire additional structural components to become infectious virions (reviewed in reference 2). Various aspects of the herpesvirus infectious cycle have been studied by live-cell microscopy using viruses encoding fluorescent-protein fusions. In particular, fusions with the capsid proteins VP26 and pUL25 are used to study capsid transport, intranuclear capsid dynamics, and nuclear egress (reviewed in reference 3). However, these proteins are not present on procapsid progenitors (4–7). While much has been learned by transmission electron microscopy and biochemical analysis of the initial stages of capsid assembly, procapsid dynamics and maturation have been inaccessible to direct observation in living cells.

Procapsids are assembled from several viral proteins: the major capsid protein (VP5), two triplex proteins (VP19C and VP23), the unique portal vertex protein (pUL6), and the large and small internal scaffolding proteins (pUL26 and pUL26.5, respectively). Once assembled, proteolytic activity embedded in the large scaffold protein triggers angularization of the capsid shell by severing the scaffold-capsid interaction (5, 8, 9). Concurrent with capsid angularization, the pUL15/pUL28/pUL33 heterotrimeric terminase complex replaces the fragmented scaffold with the linear dsDNA viral genome (10). While the bulk of the scaffold is expelled from the capsid, the protease domain (VP24) is retained as a virion structural component (6, 11–15). The angularized capsid

surface acquires the VP26 and pUL25 accessory capsid proteins, while the terminase is lost (4–7). Three angularized capsid types accumulate in infected cell nuclei: capsids that process the scaffold but do not expel it (B capsids), capsids that expel the scaffold but do not retain the viral genome (A capsids), and genome-filled C capsids (16–18).

To visualize procapsids in living cells, we sought to fuse green fluorescent protein (GFP) with a procapsid constituent of two alpha-herpesviruses: pseudorabies virus (PRV) and herpes simplex virus 1 (HSV-1). Of several fusions engineered into PRV, only GFP fused with the protease amino terminus resulted in a viable recombinant virus. The insertion did not drastically affect HSV-1 or PRV infectivity and virulence and resulted in structural incorporation of GFP into nuclear capsids and extracellular virions. The GFP-VP24 protease fusion remained capsid associated throughout infection and was retained following arrival at the nuclear membrane. Using dual-fluorescent viruses encoding pUL25/mCherry and GFP-VP24 fusions and either a wild-type or mutant protease, procapsids in living cells were identified. Finally, the rate of pUL25/mCherry acquisition provided a measurement

TABLE 1 Recombinant viruses used in the study

Strain	RFP fusion	GFP fusion	GFP position	Additional mutation(s)	Titer (PFU/ml)	Reference
PRV-Becker					3.2×10^9	23
PRV-GS3171	mRFP1-UL35[a]	UL25/GFP	L42/L43		4.8×10^8	21
PRV-GS4284	UL25/mCherry[b]				1.2×10^9	27
PRV-GS5298		GFP-5 × G-UL26[c]	M1/G2		1.1×10^9	This study
PRV-GS5125		UL26/GFP-5 × G	M247/A248		ND[f]	This study
PRV-GS4972		UL26/GFP-SGG[d]	G420/L421		ND	This study
PRV-GS4988		UL26/5 × G-GFP-SGG	G420/L421		ND	This study
PRV-GS5093		UL26/5 × G-GFP-5 × G-DASS[e]	S503/A504		ND	This study
PRV-GS5123	UL25/mCherry	GFP-5 × G-UL26	M1/G2		5.8×10^8	This study
PRV-GS6464	UL25/mCherry	GFP-5 × G-UL26	M1/G2	ΔUL33	4.0×10^{8g}	This study
HSVF-GS4553	UL25/mCherry				1.3×10^8	20
HSVF-GS5471	UL25/mCherry	GFP-5 × G-UL26	M1/A2		9.3×10^7	This study
HSVF-GS6505	UL25/mCherry	GFP-5 × G-UL26	M1/A2	VP24 S129P	5.7×10^{7h}	This study

[a] mRFP1 inserted at the 5′ end of the UL35 coding sequence.
[b] mCherry inserted in UL25 between codons 42 and 43 (PRV) or codons 50 and 51 (HSV-1).
[c] 5×G, Gly-Gly-Gly-Gly-Gly linker.
[d] SGG, Ser-Gly-Gly linker.
[e] The 4 amino acids upstream of the insertion site (Asp-Ala-Ser-Ser), which is a VP24 cleavage site, were duplicated downstream of the insertion.
[f] ND, not detected.
[g] Virus titer produced by a PRV UL33-complementing cell line.
[h] Virus titer produced by an HSV-1 UL26-complementing cell line.

of capsid angularization kinetics, which was determined to be independent of DNA encapsidation.

MATERIALS AND METHODS

Cells and viruses. Vero (African green monkey kidney epithelial), and PK15 (pig kidney epithelial) cells were maintained in Dulbecco's modified Eagle's medium (DMEM) (Invitrogen) supplemented with 10% bovine growth supplement (BGS) (HyClone). Dorsal root ganglion (DRG) primary sensory neurons were isolated from embryonic chickens (embryonic day 8) and cultured as previously described (19). A complete list of recombinant viruses used in this study is provided in Table 1, and the primers used for their production by the En Passant two-step recombination procedure are listed in Table 2. All the viruses were derived from either pBecker3 (an infectious clone of PRV strain Becker) or pYEbac102 (an infectious clone of HSV-1 strain F) (22, 23). Viruses were produced by transfection of freshly isolated infectious clone plasmids into PK15 cells (PRV) or Vero cells (HSV-1) as previously described (24). The resulting virus stocks were harvested and passaged on PK15 cells (PRV) or Vero cells (HSV-1) to generate working stocks, the titers of which were determined by plaque assay as described previously (25). The UL33-null PRV encodes a deletion of codons 27 to 46, which were replaced by 4 nucleotides (TAAA) to stop translation and place the downstream codons out of frame. The deletion was designed to preserve the overlapping promoter sequences for the neighboring UL32 and UL34 essential genes. The UL33-null virus was propagated on PK15 cells stably expressing PRV UL33 and did not produce detectable plaques on standard PK15 cells. HSV-1 encoding a S129P catalytic-inactivation mutation was propagated on Vero cells stably expressing HSV-1 UL26 (a kind gift from Fred Homa) and did not produce detectable plaques on standard Vero cells.

Virus propagation and plaque assays. Single-step growth curves were performed as previously described (26). Briefly, PK15 cells were infected with PRV at a multiplicity of infection (MOI) of 10, and cell-associated virus and supernatants were harvested at 2, 5, 8, 12, and 24 h after removal of the inoculum. The titers were quantified by plaque assay on PK15 cells. Plaque diameters were measured following infection of either Vero cells (HSV-1) or PK15 cells (PRV) in 6-well trays overlaid with 3 ml DMEM supplemented with 2% BGS and 10 mg/ml methyl cellulose. The plaques were imaged 3 or 4 days postinfection either by pUL25/mCherry fluorescence or by differential interference contrast (DIC) for viruses lacking the

pUL25 reporter fusion (wild-type PRV and PRV-GS5298). For each virus, a minimum of 75 plaques were imaged using a Nikon Eclipse TE2000-U inverted microscope. Plaque diameters were measured by drawing a diagonal line over the widest part of the plaque.

Infection of CD-1 mice. Male CD-1 mice (6 weeks old; Charles River) were maintained for at least 2 weeks (two or three mice per cage) under a 12-h/12-h light-dark (LD) cycle with food and water available *ad libitum*. Intranasal application of PRV was performed on animals anesthetized by isoflurane (2.5 to 5.0%) inhalation. Viral stocks were maintained frozen at −80°C and used immediately after being thawed. Each animal received 5 μl PRV (8×10^5 to 9×10^5 PFU) in each nostril. Behavior was continuously video monitored, and images were captured every 10 min. The time to death after inoculation was determined from recorded images and rounded to the nearest hour. All work was approved by the University of Nebraska Institutional Animal Care and Use Committee (IACUC no. 1086).

Released-particle assay. Extracellular virus particle fluorescence was analyzed by collecting supernatants from infected cells as previously described (27). Briefly, confluent Vero cells (for HSV-1) or PK15 cells (for PRV) in a 10-cm dish were infected at an MOI of 5 and incubated for 18 h in phenol red-free DMEM–F-12 medium (Gibco) supplemented with 2% (vol/vol) BGS (HyClone). The supernatant was collected and cleared of cell debris by centrifugation in a Legend XTR using a TX-750 swinging-bucket rotor (Sorvall) at 3,000 × g for 10 min at 4°C. Next, 8 ml of the cleared supernatant was transferred to an SW41 centrifuge tube and underlaid with a 1-ml cushion of 10% (wt/vol) Nycodenz (Accurate Chemical) in phosphate-buffered saline (PBS). Following centrifugation in an ultracentrifuge using an SW41 rotor (Beckman) at 38,500 × g (maximum) for 60 min at 4°C, the medium and Nycodenz cushion were removed by aspiration, and the virus pellet was resuspended in 0.1 ml PBS. The virus particles were further diluted in PBS to achieve a concentration appropriate for single-particle imaging, and 65 μl was spotted onto a plasma-cleaned no. 1.5 22- by 22-mm coverslip. Imaging was performed on an Eclipse TE2000 U wide-field fluorescence microscope fitted with a 60× 1.4-numerical-aperture (NA) objective (Nikon) and a CascadeII:512 camera (Roper Scientific).

Intranuclear-capsid isolation and analysis. PRV capsids from infected nuclei were isolated from PK15 cells at 18 h postinfection (hpi) following infection at an MOI of 10, as previously described (28). Follow-
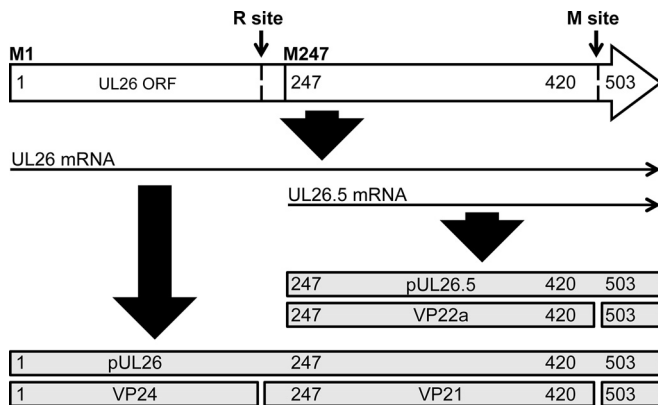
TABLE 2 Primers used to construct PRV strain Becker and HSV-1 strain F recombinants unique to the study

Strain	Template	Primer pair[a]
GS5298	pEP-EGFP-in	5′-TGAGCCCGCAGTCTCCGCGCGCGCCGCCGCCATGGTGAGCAAGGGCGAGGAG
GS5123	pEP-EGFP-in	5′-ATCGTACAGGGCCAGGTAGCCGGACACGTACACGGGCCCACCCTTGTACAGCTCGTCCATGC
GS5125	pEP-EGFP-in	5′-AGCGGGGCCTCCCGGGCCAGTGCGCCCAGTGCTGCCACCACCTCGCTGCCACCCTTGTACAGCTCGTCCATGC
GS4972	pEP-EGFP-in	5′-GAAGATGTAGTCGCCGGCGCTCGCGGGGCTCCCGGGCCTCGGGCCTGCCACCACCTCCGCCACCCTTGTACAGCTCGTCCATGC
		5′-GCCGTGCCGGGCGCTCCCGGGCCTCCAGGGCGCGAGCAAGGGCGAGGAG
GS4988	pEP-EGFP-in	5′-GACCACCTGGGCGGCGGGACGTGCCGGCGCCCAGTCCTCCTGACTTGTACAGCTCGTCCATGC
		5′-GCCGTGCCGGGCGGCGGCTCCCGGGCCTCCAGGGCGCTGCGGAGGTGGTGTGAGCAAGGGCGAGGAG
GS5093	pEP-EGFP-in	5′-CCAGCCGACGTCTCCGCCGCCACCATGACGCGGCCAGCGCCGGCGCCGGCGGCTCCCGGGCCTCCAGGGCGCTGCGGAGGAG
		5′-GGGCGCCGGCGCTGGCAGCCACGCGCCGCCGCGCCGAGGCCGCGGCTGTGAGCCGAGGCTGCGGAGGTGGTGTGAGCAAGGGCGAGGAG
GS6464	pEP-KanS2	5′-CTGCGCGGCGGATCCGAGGCCGGCGCTGAGGTGGGGAGGATCACTTCGACGTTAAACCGCGAGCTGAAAGGATGACGACGATAAGTAGGG
		5′-TAGCTTGGCGTCCGTCGTGGGGAGGATCACTTCCACCAAAGTCTCTGTGGTGCGCCATGGTGAGCAAGGGCGAGGAG
GS5471	pEP-EGFP-in	5′-GACCGTTGGGCGTTCTCCATCCGGTCTCCCGGGCATCGCGTCCACCACCTGCGCCACCCTTGTACAGCTCGTCCATGC
		5′-CAGGGGCTTCCTCCATCACCTCCTCCGTCGTGATCACCAACTACCTGCCCACAAAACGCAGGATGACGACGATAAGTAGGG
GS6505	pEP-KanS2	5′-CGCCTGTTGTACCTGATCACCAACTACCTGCCCTCCGTCGTGATCACCAACTACCTGCCCACAAAACGCAGGATGACGACGATAAGTAGGG
		5′-ATCGGGGTGCGCCTCGCCACCCAGGCGGTTTGTGCCCAGTGAGCAACCAATTCTGATTAG

[a] The underlined sequences are homologous to the plasmid template.

ing rate zonal centrifugation through a 20 to 50% sucrose gradient, three capsid species (A, B, and C) were identified as light-scattering bands and collected using a gradient fractionator (BioComp Instruments). For fluorescence microscopy experiments, the isolated capsids were spotted on glass coverslips and imaged as described for the released-particle assay. For mass spectrometry analysis, total protein from the B band was precipitated by the addition of trichloroacetic acid (TCA) to a 10% final concentration. Following a 1-h incubation on ice, samples were centrifuged in a Microfuge 18 (Beckman Coulter) at maximum speed ($18,000 \times g$) for 10 min in a 4°C refrigerator. The supernatant was aspirated, and the pellet was resuspended in protein-loading buffer (31.25 mM Tris [pH 6.8], 5% glycerol, 1% SDS, 0.005% bromophenol blue, 5% β-mercaptoethanol) supplemented with 0.1 N NaOH. Samples were then separated by SDS-PAGE, stained with Coomassie blue (Bio-Rad), destained with water, and imaged with a flat-bed scanner. The bands corresponding to VP24 (wild-type [WT] PRV) or GFP-VP24 (PRV-GS5298) were excised from the gel and submitted for mass spectrometry at the Northwestern Proteomics Core.

Mass spectrometry sample preparation. Gel slices containing protein bands were excised from an SDS-PAGE gel, diced into small pieces, destained in 500 μl of 100 mM ammonium bicarbonate (AmBic) for 1 h with shaking, and dehydrated by shaking for 10 min in 50% acetonitrile (ACN)-50% 100 mM AmBic, followed by 10 min of shaking in 100% ACN. The supernatant was then replaced with 100 μl of 10 mM dithiothreitol-100 mM AmBic. Samples were shaken at 50°C for 30 min to reduce cysteines, and the cysteine residues were subsequently alkylated with 100 μl of 100 mM iodoacetamide by incubating for 30 min in the dark at room temperature. The gel pieces were then washed in 500 μl of 50% ACN-50% 100 mM AmBic with shaking at 50°C for 45 min. Next, the gel pieces were incubated for 15 min in 100% ACN prior to drying in a vacuum concentrator and subsequently rehydrated in 100 μl of 50-ng/μl sequencing-grade trypsin (Promega, Madison, WI) in 100 mM AmBic. Samples were kept at 37°C overnight. Peptides were extracted from the gel with sequential additions of 5% ACN-0.1% formic acid (FA), 30% ACN-5% FA, and 90% ACN-5% FA. The pooled extracts were dried in a vacuum concentrator and directly resuspended in 30 μl of 5% ACN-0.1% FA for liquid chromatography-mass spectrometry (LC-MS) analysis.

LC-MS analysis. Peptides were analyzed by LC-tandem MS (MS-MS) using an Easy nanoLC-II system (Thermo Fisher Scientific) and a linear trap quadrupole (LTQ) Orbitrap Velos (Thermo Fisher Scientific) hybrid mass spectrometer. Ten-microliter injections of peptide samples were loaded onto the trap column, which was 150 μm by 3 cm self-packed with 3-μm C_{18} beads. The analytical column was a 75-μm by 10.5-cm Pico-Chip column packed with 1.9-μm C_{18} beads. The flow rate was kept at 300 nl/min. Solvent A was 0.1% FA in water, and solvent B was 0.1% FA in ACN. The gradient began at 5% B, was ramped to 35% B in 45 min and increased to 45% B over 10 min, and then was washed out at 100% B and reequilibrated to 5% B. The mass spectrometer was operated in data-dependent mode. The source voltage was 1.90 kV, and the capillary temperature was 275°C. Intact peptide mass scans (MS^1) were acquired from 400 to 2,000 m/z at 60,000 resolving power, and automatic gain control (AGC) was set to 1×10^6. The top 10 most abundant precursor ions in each MS^1 scan were selected for fragmentation. Precursors were selected with an isolation width of 1.5 Da and fragmented by collision-induced dissociation at 35% normalized collision energy, with activation Q equal to 0.250. Previously selected ions were dynamically excluded from reselection for 60 s. The fragmentation scan (MS^2) AGC was set to 3×10^4. Proteins were identified from the MS raw files using Proteome Discoverer software. MS-MS spectra were searched against the Swiss-Prot pig database, using the Sequest database search algorithm. Carbamidomethyl cysteine and oxidized methionine were set as variable modifications, and two missed tryptic cleavages were allowed. The MS^1 precursor mass tolerance was set to 10 ppm, and the MS^2 tolerance was set to 0.6 Da. A 1% false-discovery rate cutoff was applied at the peptide level. Only proteins with a

FIG 1 GFP insertions in UL26 of PRV-Becker. The UL26 open reading frame (top) is depicted, with sites of GFP insertions indicated by the preceding amino acid positions. The UL26 and UL26.5 transcripts are indicated below, followed by the encoded scaffold proteins (pUL26 and pUL26.5) and their processed forms. During capsid maturation, the N-terminal protease embedded in pUL26 cleaves at the R site in pUL26 and the M site in pUL26 and pUL26.5.

minimum of two unique peptides above the cutoff were considered for further study.

Live-cell fluorescence microscopy. To monitor GFP-VP24 and pUL25/mCherry capsid signals during infection, cells were imaged in wax-sealed chambers as previously described (19). Imaging of incoming capsids at nuclear rims was achieved 2.5 to 3.0 hpi in explanted DRGs exposed to 1×10^7 PFU per coverslip. Intranuclear-capsid assemblies were imaged following infection of Vero cells under varying conditions, as noted in the figure legends. A Ti inverted microscope fitted with 60× 1.4-NA and 100× 1.45-NA objectives (Nikon Instruments) and coupled with a CSU-W1 confocal head (Yokogawa Electric Corporation) and a CascadeII:1024 EM-CCD (Photometrics) was housed in a environmental box set to 37°C (InVivo Scientific). Illumination was provided by Obis 488 and Sapphire 561 lasers (Coherent) and custom laser launch (Solamere Technology Group, Inc.).

RESULTS

Fusion of the green fluorescent protein with the maturation protease. To visualize procapsids in living cells, we produced a series of GFP fusions with the procapsid scaffold and the maturation protease of PRV. Similar to those of HSV-1, the PRV scaffold proteins (pUL26 and pUL26.5) are encoded by two overlapping genes, UL26 and UL26.5, so that the UL26.5 open reading frame (ORF) is in frame with and corresponds to the 3′ portion of UL26 (29, 30). The VP24 maturation protease is housed in the amino terminus of pUL26 and upon activation autocatalytically releases from the scaffold backbone by cleavage at its release (R) site (30–32). VP24 also severs both scaffold proteins from the interior surface of the capsid shell by cleavage at the maturation (M) site (31). The resulting VP21 and VP22a products are expelled from the capsid, while VP24 and, presumably, a 25-amino-acid C-terminal scaffold fragment remain as structural components (11–15, 33–35). Based on these findings, four fusions were designed to position GFP at the N terminus of the protease, at the N terminus of pUL26.5, near the C terminus of VP21/VP22a, and in the pUL26/pUL26.5 C-terminal fragment (Fig. 1 and Table 1).

The GFP coding sequence was introduced into an infectious clone of PRV strain Becker, and the resulting constructs were transfected into pig kidney epithelial (PK15) cells to produce virus stocks (23). Of the four recombinant viruses, only PRV encoding GFP fused to the amino terminus of the VP24 protease (GFP-VP24) proved viable. A dual-fluorescent variant of the GFP-VP24 virus that also encodes a pUL25/mCherry fusion, which tags capsids with red fluorescence following scaffold proteolytic processing, was produced to assist with analysis of capsid maturation (see below) (27, 36). Fusion of GFP to the amino terminus of VP24 did not substantially impair the single-step growth kinetics of PRV (Fig. 2A), although a small reduction in virulence was noted based on the mean survival time following intranasal installation of CD-1 mice that was on par with that of a traditional GFP-VP26 capsid reporter virus (Fig. 2B) (19). Based on these encouraging results, an HSV-1 strain F recombinant encoding the equivalent pUL25/mCherry and GFP-VP24 fusions was produced. The plaque diameters of the HSV-1 and PRV recombinants were within 15% of those of the parental strains (Fig. 2C), and the final titers approximated those of the respective parental strains (Table 1). Taken together, these data indicated that inserting GFP at the amino terminus of the VP24 maturation protease was tolerated by the viruses.

GFP-VP24 incorporation into capsids and virions. The VP24 maturation protease is a component of all capsid species, either as a fusion to the scaffold (procapsids) (5, 9, 37), as a liberated peptide within A, B, and C (A/B/C) capsids isolated from infected cell nuclei (11, 13, 33, 37), or in capsids isolated from extracellular virus particles. The copy number of VP24 in B capsids is estimated at 147 (38), which can be extrapolated to all capsid species, as the protease content does not substantially vary between them (16, 33, 39). To determine the copy number of the GFP-VP24 fusion, nuclear A, B, and C capsids were separated on 20 to 50% sucrose gradients following their isolation from PK15 cells infected with PRV encoding either unmodified or GFP-tagged VP24 (28). The integrity of the GFP-VP24 polypeptide incorporated into capsids was confirmed by Western blotting with an anti-GFP antibody (data not shown). The protein composition of the B capsids was first analyzed by SDS-PAGE, followed by Coomassie blue staining. Wild-type VP24 was detected as a 27-kDa species (39), which was replaced by an ∼50-kDa band in B capsids isolated from the GFP-VP24 virus (Fig. 3A). The identities of the VP24 and GFP-VP24 bands were confirmed by mass spectrometry (see Tables S1 and S2 in the supplemental material). Next, GFP emissions from individual capsids were measured by spotting the capsids on glass coverslips and imaging by quantitative fluorescence microscopy. The distribution of diffraction-limited fluorescence intensities was Gaussian for the three capsid types, consistent with copy-controlled incorporation of GFP-VP24 (Fig. 3B) (21). To determine the copy number of GFP-VP24 per capsid, a GFP emission profile from a pUL25/GFP-encoding PRV recombinant was used as a standard (PRV-GS3171) (Table 1). We had previously determined that pUL25/GFP fusions are copy controlled at approximately 70.5 copies per capsid (21). In comparison, GFP-VP24 was present at approximately 25 copies per capsid for the three capsid types (Fig. 3C). This level of incorporation was 6-fold lower than expected (38), which was consistent with reduced incorporation of the GFP fusion observed on denaturing gels (Fig. 3A). The cause of this reduction is not immediately clear but may have resulted from steric hindrance within the crowded scaffold environment combined with the flexibility of the scaffold to use reduced amounts of pUL26 during assembly (40).

Extracellular dual-fluorescent HSV-1 and PRV particles were isolated from the supernatants of infected cells at 18 hpi
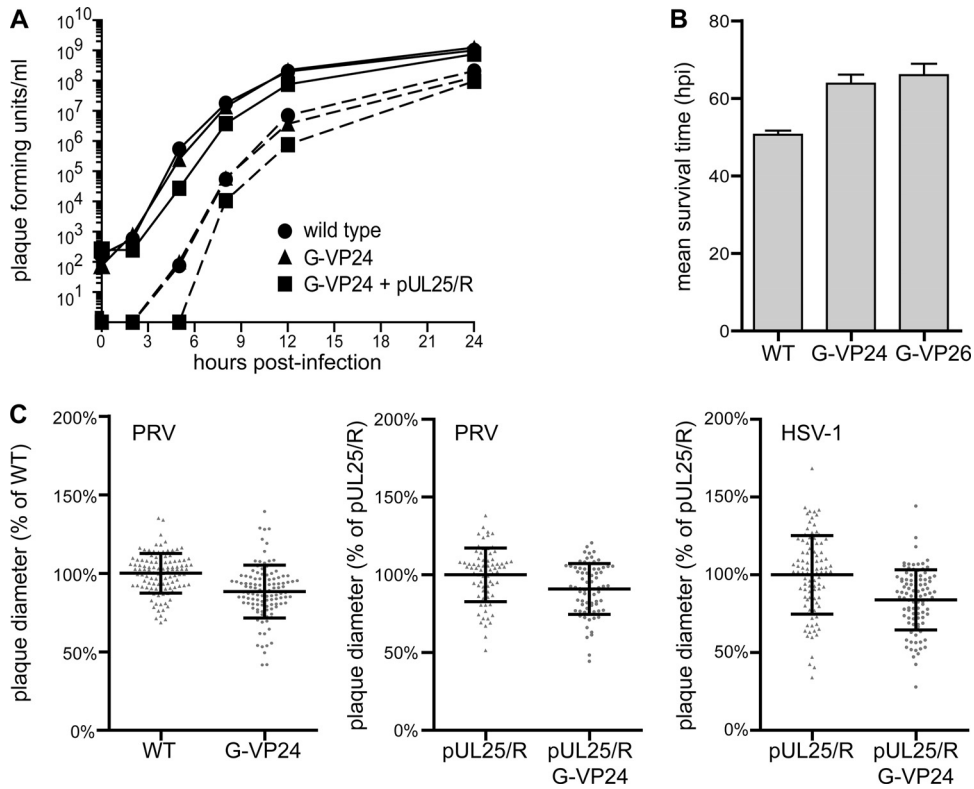
FIG 2 Propagation of PRV and HSV-1 encoding a GFP fusion with the amino terminus of VP24. (A) Single-step growth kinetics of WT, GFP-VP24 (G-VP24), and dual-fluorescent PRV. The dual-fluorescent virus encodes GFP-VP24 and a UL25/mCherry (UL25/R) capsid reporter. Viruses were harvested from adherent PK15 cells (solid lines) or infected cell supernatants (dashed lines), and titers were determined by plaque assay. (B) Virulence of PRV recombinants following intranasal installation in CD-1 mice. PRV encoding a traditional GFP-VP26 capsid fusion is included for comparison ($n = 5$ per group). (C) Plaque diameters of PRV and HSV-1 recombinant viruses. The diameters of individual plaques are expressed as percentages of either WT or pUL25/mCherry viruses, as indicated. The error bars indicate standard deviations (SD).

and spotted on coverslips for analysis, as described above. The particles displayed coincident GFP-VP24 and pUL25/mCherry signals, as was expected for these two copy-controlled structural proteins (Fig. 4A). As with capsids isolated from nuclei, the GFP emissions from the extracellular particles had a Gaussian distribution, with the specific GFP-VP24 incorporation into PRV and HSV-1 virions equivalent to the copy numbers calculated for nuclear capsids (Fig. 4B and C). These results also indicated that the pUL25/mCherry fusion did not alter GFP-VP24 occupation.
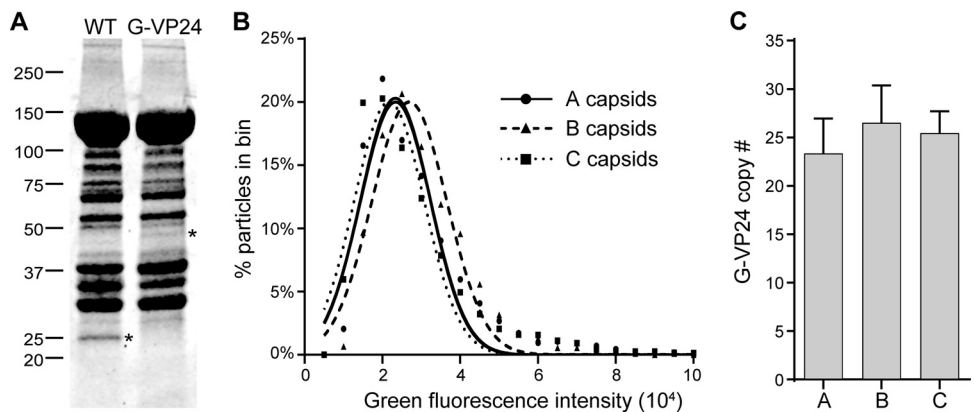
FIG 3 GFP-VP24 incorporation in PRV capsids isolated from infected cell nuclei. (A) Proteins from WT and GFP-VP24 (G-VP24) B capsids were separated by SDS-PAGE and stained with Coomassie blue. The protein bands corresponding to VP24 and GFP-VP24 are indicated by asterisks. Numbers on the left indicate molecular mass in kilodaltons. (B) Frequency distributions of green-fluorescence intensities (arbitrary units) in nuclear capsid populations. Each population was fit by a normal distribution using nonlinear regression ($R^2 \geq 0.90$ for each population). (C) VP24 copy numbers in A, B, and C capsid populations were determined by dividing the VP24 mean fluorescence intensity by the mean fluorescence of PRV encoding a pUL25/GFP capsid fusion and multiplied by the estimated copy number of pUL25/GFP (see the text). The error bars indicate standard errors of the mean (SEM) based on four independent experiments.
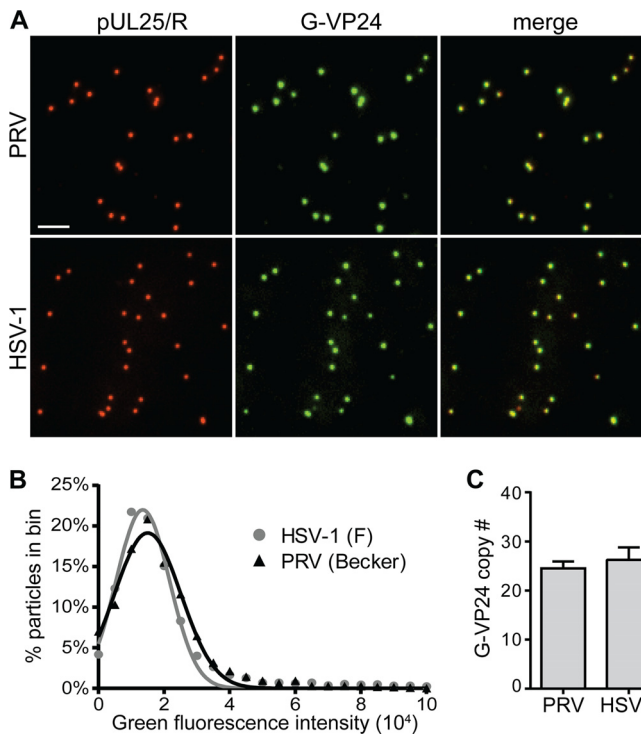
FIG 4 GFP-VP24 copy numbers in PRV and HSV-1 extracellular particles. (A) Images of dual-fluorescent extracellular virus particles encoding GFP-VP24 (G-VP24) and pUL25/mCherry (pUL25/R). Scale bar = 2 μm. (B) Frequency distributions of green fluorescence intensities. Both viruses were modeled by normal distributions ($R^2 = 0.98$ for PRV and HSV-1 populations). (C) The GFP-VP24 copy number was determined as described for Fig. 3. The error bars indicate SEM based on four independent experiments.

FIG 5 GFP-VP24 remains capsid associated following infection. Shown are representative images of dorsal root ganglion sensory neuron nuclei following infection with dual-fluorescence PRV or HSV-1 encoding GFP-VP24 (G-VP24) and pUL25/mCherry (pUL25/R) at 2.5 hpi. The mCherry/pUL25-tagged incoming capsids lining the nuclear rims show coincident GFP-VP24 signal. Scale bar = 5 μm.

GFP-VP24 is retained in capsids following entry into cells. Although the VP24 protease is a component of extracellular viral particles, whether the protease is retained following entry into cells and during capsid delivery to nuclear pores is unknown. To examine the GFP-VP24 content of intracellular capsids, the nuclei of primary sensory neurons were imaged following infection with dual-fluorescent HSV-1 or PRV encoding GFP-VP24 and pUL25/mCherry. Capsids at the nuclear rim were consistently positive for both fluorescent signals, indicating that GFP-VP24 remains capsid associated following entry into cells and was evidently not injected into nuclei (Fig. 5). Diffuse intranuclear fluorescence was also observed to various degrees, likely resulting from *de novo* protein synthesis.

Identifying procapsids in living cells. The addition of the pUL25 and VP26 proteins to the capsid surface occurs upon scaffold cleavage and concurrent angularization of the capsid shell (4–7). Therefore, pUL25 and VP26 are markers of A/B/C capsids that are restricted from procapsids. Both of these proteins are traditionally used to label capsids with fluorescent protein fusions, with pUL25 being particularly tolerant of such reporters (27, 36, 41). In contrast, the GFP-VP24 fusion was expected to label all capsid species, including procapsids. As a first step to determining if procapsids were labeled, a VP24 S129P codon change was introduced into the dual-fluorescent HSV-1 to disrupt the active-site nucleophile and thereby catalytically inactivate the protease (42, 43). Inactivation of the protease renders HSV-1 unable to trigger procapsid maturation, and consistent with this, the S129P virus
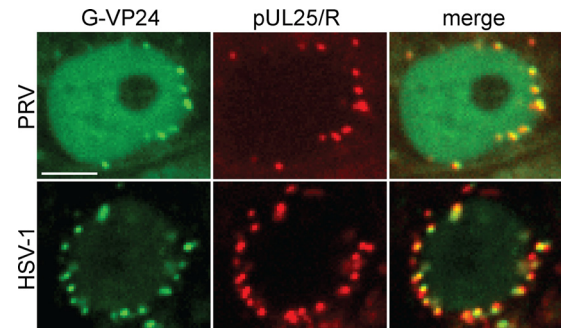
could be propagated only on a *trans*-complementing cell line that expressed wild-type pUL26 (Table 1) (42, 44). Following infection of noncomplementing cells, GFP-VP24 diffraction-limited punctae were readily observed within infected cell nuclei, and these structures uniformly lacked red fluorescence (Fig. 6). Occasional dual-fluorescent punctae detected at the nuclear periphery that were consistent with the input capsids that initiated the infection were observed. The GFP-VP24 particles displayed random motion in the nucleus similar to that described for angularized capsids labeled with GFP-VP26 fusions (see Movie S1 in the supplemental material) (45).

Because GFP-VP24 assembled into diffraction-limited structures in the absence of a catalytically active maturation protease, we next examined whether these structures were discernible during infection with virus encoding wild-type protease and if the particles acquired the pUL25/mCherry maturation marker. At 6 h postinfection, punctate GFP-VP24 emission profiles were again detected in the absence of pUL25/mCherry signal. As the infection progressed over the next 2 h, many of the GFP-VP24 emission sources became coincident with pUL25/mCherry signal (Fig. 7). This protease-dependent acquisition of the pUL25/mCherry capsid shell maturation marker was consistent with the GFP-VP24 emission sources being procapsids. For both HSV-1 and PRV, the sites of capsid maturation were distributed throughout the nucleus. Taken together, these observations indicate that GFP-VP24 is a pancapsid marker that allows visualization of procapsids and their morphogenesis.

The herpesvirus terminase does not enhance capsid angularization. An unexpected aspect of herpesvirus capsid maturation is the apparently low efficiency of the process. Many capsids isolated from the nuclei of cells infected with HSV-1 and PRV have a cleaved scaffold and lack encapsidated viral genomes (i.e., B capsids) (16, 28, 46). This inefficiency can be accounted for, at least in part, by the finding that terminase mutant viruses produce abundant B capsids, which indicates that VP24 can activate in the absence of genome encapsidation (47–51). Whether genome-containing C capsids are the products of chance events that saw terminase and protease activities triggered concurrently or whether terminase can enhance protease activation to help promote a coupled scaffold-genome exchange is unknown. Using the dual-fluorescent PRV, the ki-
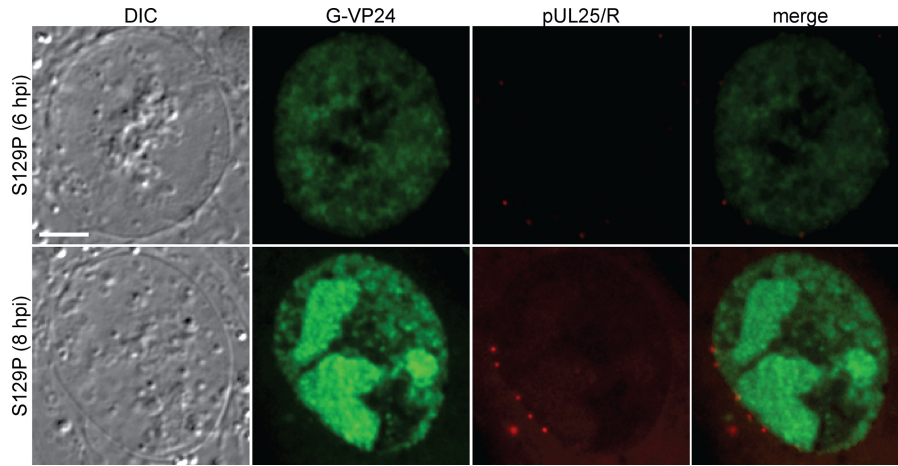
FIG 6 Visualizing procapsids in living cells. Vero cells were infected with HSV-1 encoding a catalytically inactive protease (S129P) at an MOI of 6 and imaged by confocal microscopy. Large populations of GFP-VP24-emitting particles were visible in nuclei by 6 hpi (top) and continued to accumulate by 8 hpi (bottom). The pUL25/mCherry fluorescence indicative of mature capsids was confined to the initial incoming capsids at the nuclear rims. Scale bar = 5 μm.

netics of pUL25/mCherry acquisition and its dependence upon encapsidation were assessed in the presence (WT UL33) and absence (ΔUL33) of a functional terminase complex (28, 48, 51). UL33 encodes an essential component of the viral termi-

nase that packages the viral genome into capsids; as such, PRV with UL33 deleted could be propagated only on a *trans*-complementing cell line (Table 1). Infections with WT UL33 and ΔUL33 dual-fluorescent PRV were monitored every 5 min be-
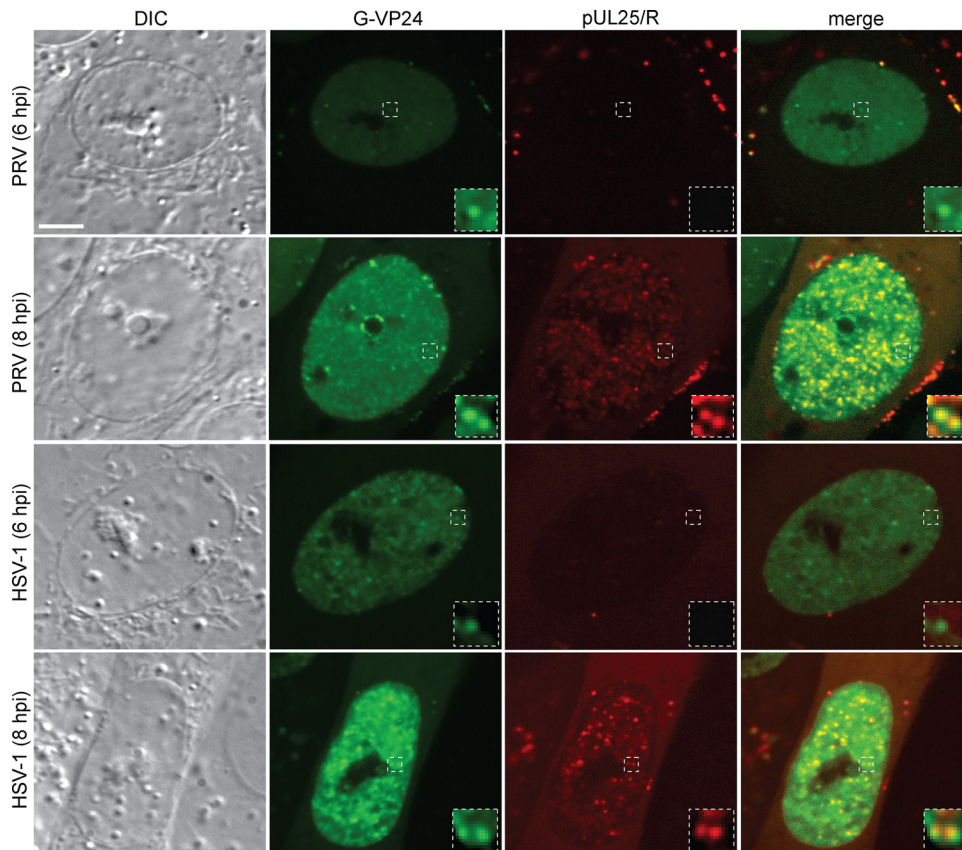
FIG 7 Monitoring capsid maturation with dual-fluorescent viruses. Cells were infected with PRV or HSV-1 encoding GFP-VP24 (G-VP24) and pUL25/mCherry (pUL25/R) at an MOI of 10 and imaged at 6 and 8 hpi by confocal microscopy. All the GFP-VP24 images are scaled equivalently to show relative fluorescence intensities, as are the pUL25/mCherry images. The insets provide enlargements of intranuclear particles that produced diffraction-limited emissions consistent with procapsids (GFP only) and angularized capsids (GFP/mCherry dual fluorescence). The insets are scaled to improve the contrast of individual particles. Scale bar = 5 μm.
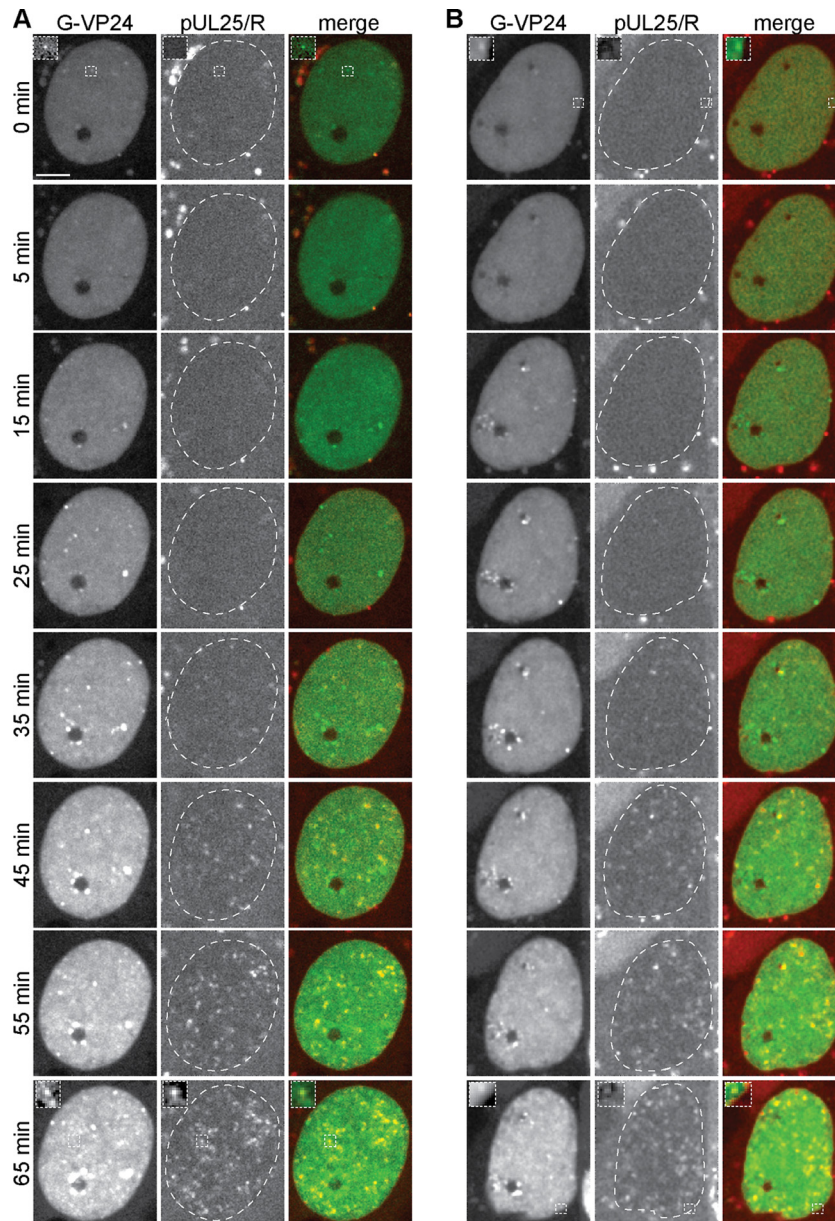
FIG 8 Encapsidation does not enhance capsid shell maturation kinetics. Vero cells were infected with PRV encoding GFP-VP24 (G-VP24) and pUL25/mCherry (pUL25/R) and either wild-type UL33 (A) or ΔUL33 (B) at an MOI of 20. Individual nuclei were continuously imaged by confocal microscopy at 5-min intervals beginning at approximately 5 hpi. The indicated time points of representative recordings are presented (five cells were recorded per virus). The insets (0 min and 65 min) were scaled to improve the contrast of individual particles. Scale bar = 5 μm.

ginning at 5 h postinfection. For each infection, the time between the first appearance of GFP-VP24 intranuclear punctae and the onset of pUL25/mCherry acquisition was determined. GFP-VP24 punctae generally persisted for 35 min prior to acquisition of the pUL25/mCherry maturation marker, and this period was not detectably impacted by the absence of a functional terminase (Fig. 8).

DISCUSSION

Herpesvirus capsid assembly and maturation have long been considered targets for antiviral development, and significant efforts have been applied to understand this fundamental aspect of infec-

tion. Several approaches have provided important insights into these processes, including analysis of temperature-sensitive assembly defects (4, 6, 9, 10, 40, 47), reconstitution of capsid assembly by baculovirus expression (37, 52–54), and three-dimensional reconstruction of capsid intermediates by cryo-electron microscopy (5, 8, 17, 55–61). Collectively, these studies have helped define the procapsid precursor and its three maturation products: A, B, and C capsids. By transmission electron microscopy, the procapsid appears as a 125-nm shell containing a large concentric core, which collapses to a small core following scaffold cleavage (16, 18, 62). Thus, HSV-1 encoding temperature-sensitive mutations in the maturation protease produces only large-core capsids

at nonpermissive temperatures (9, 10, 47). Production of C capsids consists of at least two maturation events that are closely coupled: capsid shell angularization and genome encapsidation (17, 18, 63). Little is known regarding the circumstances that govern these events, and this has in part been due to an inability to monitor procapsids in living cells. Whereas imaging of fluorescent reporter viruses has been instrumental in studying many aspects of the herpesvirus infectious cycle, studying the dynamics of capsid assembly and morphogenesis has been constrained by the lack of a suitable reporter design that provides for procapsid imaging.

Two approaches have proven effective in imaging capsids in living cells. Tagging either the VP26 hexon tip protein (64) or the pUL25 outer penton protein (36, 41) with a fluorescent protein results in fluorescent capsids that allow imaging and tracking of individual particles in cells. The high copy number of VP26 provides bright fluorescent emissions when fused with a fluorescent protein but can impair aspects of herpesvirus infection (65, 66), whereas fusion with pUL25 yields 4-fold-dimmer fluorescence emissions than an equivalent VP26 reporter and is less detrimental to the virus (27). However, neither of these proteins is useful for labeling of procapsids, as both are added to the outer capsid shell upon its angularization, which is triggered by internal scaffold cleavage (4–7). Therefore, VP26 and pUL25 are markers of capsids that have a mature shell, which include A, B, and C capsids isolated from infected cell nuclei and C capsids isolated from extracellular virions (6, 7, 12, 14, 38, 67). To image the procapsid progenitor, we made recombinants of PRV that encode GFP fused to different regions of the pUL26/pUL26.5 scaffold proteins. While the majority of these designs were lethal to PRV, we report the construction and analysis of recombinant PRV and HSV-1 with GFP fused to the VP24 maturation protease that maintained nearly wild-type infectivity.

Fusing GFP to VP24 achieves two useful advances. First, unlike fusions to VP26 and pUL25, which decorate the capsid surface with GFP, the fluorescent protein is contained within the capsid shell. By leaving the outer capsid surface free of GFP decoration, capsid interactions with many cellular and viral factors should remain unperturbed. Second, the GFP-VP24 fusion makes the procapsid accessible to studies of its dynamics and maturation in living cells. To confirm that the GFP-VP24 reporter fusion provided a reliable procapsid signal, a virus encoding GFP-VP24 and pUL25/mCherry was produced, with the expectation that procapsids would emit green, but not red, fluorescence. This virus was further altered to encode a catalytically inactive protease (S129P mutation in VP24) to prevent procapsid maturation (42, 44). Consistent with expectations, green-fluorescent diffraction-limited intranuclear punctae became prevalent in the nuclei of infected cells, and these structures failed to acquire red fluorescence. These particles exhibited random motion, similar to a report of angularized capsids (45). In contrast, the pUL25/mCherry signal was acquired by green-fluorescent particles in the presence of a wild-type protease. These observations authenticate the GFP-VP24 fusion as a procapsid reporter and demonstrate the utility of the fusion in visualizing procapsids in living cells. It should be emphasized, however, that GFP-VP24 is not specific to procapsids but rather labels all capsid species.

The copy number of the VP24 protease in B capsids was previously estimated at 147 copies by densitometric analysis of Coomassie blue-stained SDS-PAGE gels (38). Because procapsids are unstable when isolated from nuclei (5), fluorescent emissions were measured from purified A/B/C capsids and virions to determine the GFP-VP24 copy number, which approximated 25 copies/capsid. We note that this value is 6-fold lower than expected, which was supported by our Coomassie blue analysis of B capsid composition. Therefore, we conclude that the copy number of GFP in the capsid interior is likely limited by the crowded environment. This is a noteworthy constraint, considering the use of this fusion in studies of scaffold assembly. Despite the decreased copy number of pUL26, the GFP-VP24 reporter was tolerated by HSV-1 and PRV remarkably well. Tagging VP24 with GFP did not impair single-step growth of PRV, and decreases in plaque diameter and virulence in a mouse model were statistically significant but not severe.

Using the dual-fluorescent recombinants of PRV encoding GFP-VP24 and pUL25/mCherry, procapsids were consistently detected in infected cell nuclei approximately 35 min before association with the pUL25/mCherry marker became evident. This maturation time was consistent with a previous estimate based on HSV-1 encoding a temperature-sensitive protease and the detection of capsid angularization using a conformation-specific antibody (10). There was no obvious preferential site for procapsid assembly or maturation, as both processes appeared to occur randomly throughout the interior of the nucleus. Although genome encapsidation is not a prerequisite for capsid angularization, we were curious if the former promotes the latter, as such a scenario would help favor the production of C capsids. Within the resolution limits of the assay, this proved not to be the case; procapsids of a terminase mutant virus (UL33 null) acquired the pUL25/mCherry maturation marker at the same rate as wild-type virus. These results indicate that the rates of protease activation, scaffold cleavage, and capsid angularization were not measurably reduced in the absence of a functional terminase. The finding is consistent with the high yield of B capsids normally obtained from cells infected with wild-type HSV-1 and PRV and suggests that successful encapsidation may require fortuitous timing of encapsidation and scaffold cleavage. Alternatively, during wild-type infections, some encapsidation events may be coupled with nuclear egress, with the resulting C capsids being rapidly lost from the intranuclear-capsid population.

In summary, this study describes recombinant PRV and HSV-1 expressing a fluorescent-protein fusion with a core protein present in procapsids, as well as all other capsid species, which is therefore the first herpesvirus pancapsid live-cell marker. The approach makes investigation of capsid assembly, maturation, encapsidation, nuclear egress, and the coordination of these processes accessible in living cells. Our initial application of this technology reveals procapsids to be dynamic particles that exhibit random intranuclear motion and maturation kinetics that are independent of genome encapsidation.

ACKNOWLEDGMENTS

REFERENCES

1. **Cardone G, Heymann JB, Cheng N, Trus BL, Steven AC.** 2012. Procapsid assembly, maturation, nuclear exit: dynamic steps in the production of infectious herpesvirions. Adv Exp Med Biol **726:**423–439. http://dx.doi.org/10.1007/978-1-4614-0980-9_19.
2. **Mettenleiter TC, Klupp BG, Granzow H.** 2009. Herpesvirus assembly: an update. Virus Res **143:**222–234. http://dx.doi.org/10.1016/j.virusres.2009.03.018.
3. **Hogue IB, Bosse JB, Engel EA, Scherer J, Hu JR, Del Rio T, Enquist LW.** 2015. Fluorescent protein approaches in alpha herpesvirus research. Viruses **7:**5933–5961. http://dx.doi.org/10.3390/v7112915.
4. **Chi JH, Wilson DW.** 2000. ATP-dependent localization of the herpes simplex virus capsid protein VP26 to sites of procapsid maturation. J Virol **74:**1468–1476. http://dx.doi.org/10.1128/JVI.74.3.1468-1476.2000.
5. **Newcomb WW, Trus BL, Cheng N, Steven AC, Sheaffer AK, Tenney DJ, Weller SK, Brown JC.** 2000. Isolation of herpes simplex virus procapsids from cells infected with a protease-deficient mutant virus. J Virol **74:**1663–1673. http://dx.doi.org/10.1128/JVI.74.4.1663-1673.2000.
6. **Sheaffer AK, Newcomb WW, Gao M, Yu D, Weller SK, Brown JC, Tenney DJ.** 2001. Herpes simplex virus DNA cleavage and packaging proteins associate with the procapsid prior to its maturation. J Virol **75:**687–698. http://dx.doi.org/10.1128/JVI.75.2.687-698.2001.
7. **Thurlow JK, Rixon FJ, Murphy M, Targett-Adams P, Hughes M, Preston VG.** 2005. The herpes simplex virus type 1 DNA packaging protein UL17 is a virion protein that is present in both the capsid and the tegument compartments. J Virol **79:**150–158. http://dx.doi.org/10.1128/JVI.79.1.150-158.2005.
8. **Newcomb WW, Homa FL, Thomsen DR, Booy FP, Trus BL, Steven AC, Spencer JV, Brown JC.** 1996. Assembly of the herpes simplex virus capsid: characterization of intermediates observed during cell-free capsid formation. J Mol Biol **263:**432–446. http://dx.doi.org/10.1006/jmbi.1996.0587.
9. **Rixon FJ, McNab D.** 1999. Packaging-competent capsids of a herpes simplex virus temperature-sensitive mutant have properties similar to those of in vitro-assembled procapsids. J Virol **73:**5714–5721.
10. **Church GA, Wilson DW.** 1997. Study of herpes simplex virus maturation during a synchronous wave of assembly. J Virol **71:**3603–3612.
11. **Stevenson AJ, Morrison EE, Chaudhari R, Yang CC, Meredith DM.** 1997. Processing and intracellular localization of the herpes simplex virus type 1 proteinase. J Gen Virol **78:**671–675. http://dx.doi.org/10.1099/0022-1317-78-3-671.
12. **Loret S, Guay G, Lippe R.** 2008. Comprehensive characterization of extracellular herpes simplex virus type 1 virions. J Virol **82:**8605–8618. http://dx.doi.org/10.1128/JVI.00904-08.
13. **Person S, Desai P.** 1998. Capsids are formed in a mutant virus blocked at the maturation site of the UL26 and UL26.5 open reading frames of herpes simplex virus type 1 but are not formed in a null mutant of UL38 (VP19C). Virology **242:**193–203. http://dx.doi.org/10.1006/viro.1997.9005.
14. **Kramer T, Greco TM, Enquist LW, Cristea IM.** 2011. Proteomic characterization of pseudorabies virus extracellular virions. J Virol **85:**6427–6441. http://dx.doi.org/10.1128/JVI.02253-10.
15. **Spear PG, Roizman B.** 1972. Proteins specified by herpes simplex virus. V. Purification and structural proteins of the herpesvirion. J Virol **9:**143–159.
16. **Gibson W, Roizman B.** 1972. Proteins specified by herpes simplex virus. 8. Characterization and composition of multiple capsid forms of subtypes 1 and 2. J Virol **10:**1044–1052.
17. **Booy FP, Newcomb WW, Trus BL, Brown JC, Baker TS, Steven AC.** 1991. Liquid-crystalline, phage-like packing of encapsidated DNA in herpes simplex virus. Cell **64:**1007–1015. http://dx.doi.org/10.1016/0092-8674(91)90324-R.
18. **Perdue ML, Cohen JC, Kemp MC, Randall CC, O'Callaghan DJ.** 1975. Characterization of three species of nucleocapsids of equine herpesvirus type-1 (EHV-1). Virology **64:**187–204. http://dx.doi.org/10.1016/0042-6822(75)90091-4.
19. **Smith GA, Gross SP, Enquist LW.** 2001. Herpesviruses use bidirectional fast-axonal transport to spread in sensory neurons. Proc Natl Acad Sci U S A **98:**3466–3470. http://dx.doi.org/10.1073/pnas.061029798.
20. **Huffmaster NJ, Sollars PJ, Richards AL, Pickard GE, Smith GA.** 2015. Dynamic ubiquitination drives herpesvirus neuroinvasion. Proc Natl Acad Sci U S A **112:**12818–12823. http://dx.doi.org/10.1073/pnas.1512559112.
21. **Bohannon KP, Jun Y, Gross SP, Smith GA.** 2013. Differential protein partitioning within the herpesvirus tegument and envelope underlies a complex and variable virion architecture. Proc Natl Acad Sci U S A **110:**E1613–E1620. http://dx.doi.org/10.1073/pnas.1221896110.
22. **Tanaka M, Kagawa H, Yamanashi Y, Sata T, Kawaguchi Y.** 2003. Construction of an excisable bacterial artificial chromosome containing a full-length infectious clone of herpes simplex virus type 1: viruses reconstituted from the clone exhibit wild-type properties in vitro and in vivo. J Virol **77:**1382–1391. http://dx.doi.org/10.1128/JVI.77.2.1382-1391.2003.
23. **Smith GA, Enquist LW.** 2000. A self-recombining bacterial artificial chromosome and its application for analysis of herpesvirus pathogenesis. Proc Natl Acad Sci U S A **97:**4873–4878. http://dx.doi.org/10.1073/pnas.080502497.
24. **Luxton GW, Haverlock S, Coller KE, Antinone SE, Pincetic A, Smith GA.** 2005. Targeting of herpesvirus capsid transport in axons is coupled to association with specific sets of tegument proteins. Proc Natl Acad Sci U S A **102:**5832–5837. http://dx.doi.org/10.1073/pnas.0500803102.
25. **Antinone SE, Smith GA.** 2010. Retrograde axon transport of herpes simplex virus and pseudorabies virus: a live-cell comparative analysis. J Virol **84:**1504–1512. http://dx.doi.org/10.1128/JVI.02029-09.
26. **Tirabassi RS, Enquist LW.** 1998. Role of envelope protein gE endocytosis in the pseudorabies virus life cycle. J Virol **72:**4571–4579.
27. **Bohannon KP, Sollars PJ, Pickard GE, Smith GA.** 2012. Fusion of a fluorescent protein to the pUL25 minor capsid protein of pseudorabies virus allows live-cell capsid imaging with negligible impact on infection. J Gen Virol **93:**124–129. http://dx.doi.org/10.1099/vir.0.036145-0.
28. **Leelawong M, Guo D, Smith GA.** 2011. A physical link between the pseudorabies virus capsid and the nuclear egress complex. J Virol **85:**11675–11684. http://dx.doi.org/10.1128/JVI.05614-11.
29. **Dezelee S, Bras F, Vende P, Simonet B, Nguyen X, Flamand A, Masse MJ.** 1996. The BamHI fragment 9 of pseudorabies virus contains genes homologous to the UL24, UL25, UL26, and UL 26.5 genes of herpes simplex virus type 1. Virus Res **42:**27–39. http://dx.doi.org/10.1016/0168-1702(96)01293-2.
30. **Liu FY, Roizman B.** 1991. The herpes simplex virus 1 gene encoding a protease also contains within its coding domain the gene encoding the more abundant substrate. J Virol **65:**5149–5156.
31. **DiIanni CL, Drier DA, Deckman IC, McCann PJ, III, Liu F, Roizman B, Colonno RJ, Cordingley MG.** 1993. Identification of the herpes simplex virus-1 protease cleavage sites by direct sequence analysis of autoproteolytic cleavage products. J Biol Chem **268:**2048–2051.
32. **Weinheimer SP, McCann PJ III, O'Boyle DR, II, Stevens JT, Boyd BA, Drier DA, Yamanaka GA, DiIanni CL, Deckman IC, Cordingley MG.** 1993. Autoproteolysis of herpes simplex virus type 1 protease releases an active catalytic domain found in intermediate capsid particles. J Virol **67:**5813–5822.
33. **Sheaffer AK, Newcomb WW, Brown JC, Gao M, Weller SK, Tenney DJ.** 2000. Evidence for controlled incorporation of herpes simplex virus type 1 UL26 protease into capsids. J Virol **74:**6838–6848. http://dx.doi.org/10.1128/JVI.74.15.6838-6848.2000.
34. **Hong Z, Beaudet-Miller M, Durkin J, Zhang R, Kwong AD.** 1996. Identification of a minimal hydrophobic domain in the herpes simplex virus type 1 scaffolding protein which is required for interaction with the major capsid protein. J Virol **70:**533–540.
35. **Desai P, Person S.** 1996. Molecular interactions between the HSV-1 capsid proteins as measured by the yeast two-hybrid system. Virology **220:**516–521. http://dx.doi.org/10.1006/viro.1996.0341.
36. **Conway JF, Cockrell SK, Copeland AM, Newcomb WW, Brown JC, Homa FL.** 2010. Labeling and localization of the herpes simplex virus capsid protein UL25 and its interaction with the two triplexes closest to the penton. J Mol Biol **397:**575–586. http://dx.doi.org/10.1016/j.jmb.2010.01.043.
37. **Tatman JD, Preston VG, Nicholson P, Elliott RM, Rixon FJ.** 1994. Assembly of herpes simplex virus type 1 capsids using a panel of recombinant baculoviruses. J Gen Virol **75:**1101–1113. http://dx.doi.org/10.1099/0022-1317-75-5-1101.
38. **Newcomb WW, Trus BL, Booy FP, Steven AC, Wall JS, Brown JC.** 1993.

Structure of the herpes simplex virus capsid. Molecular composition of the pentons and the triplexes. J Mol Biol **232:**499–511.

39. **Homa FL, Huffman JB, Toropova K, Lopez HR, Makhov AM, Conway JF.** 2013. Structure of the pseudorabies virus capsid: comparison with herpes simplex virus type 1 and differential binding of essential minor proteins. J Mol Biol **425:**3415–3428. http://dx.doi.org/10.1016/j.jmb.2013.06.034.

40. **Gao M, Matusick-Kumar L, Hurlburt W, DiTusa SF, Newcomb WW, Brown JC, McCann PJ, III, Deckman I, Colonno RJ.** 1994. The protease of herpes simplex virus type 1 is essential for functional capsid formation and viral growth. J Virol **68:**3702–3712.

41. **Cockrell SK, Sanchez ME, Erazo A, Homa FL.** 2009. Role of the UL25 protein in herpes simplex virus DNA encapsidation. J Virol **83:**47–57. http://dx.doi.org/10.1128/JVI.01889-08.

42. **DiIanni CL, Stevens JT, Bolgar M, O'Boyle DR, II, Weinheimer SP, Colonno RJ.** 1994. Identification of the serine residue at the active site of the herpes simplex virus type 1 protease. J Biol Chem **269:**12672–12676.

43. **Hoog SS, Smith WW, Qiu X, Janson CA, Hellmig B, McQueney MS, O'Donnell K, O'Shannessy D, DiLella AG, Debouck C, Abdel-Meguid SS.** 1997. Active site cavity of herpesvirus proteases revealed by the crystal structure of herpes simplex virus protease/inhibitor complex. Biochemistry **36:**14023–14029. http://dx.doi.org/10.1021/bi9712697.

44. **Robertson BJ, McCann PJ, III, Matusick-Kumar L, Newcomb WW, Brown JC, Colonno RJ, Gao M.** 1996. Separate functional domains of the herpes simplex virus type 1 protease: evidence for cleavage inside capsids. J Virol **70:**4317–4328.

45. **Bosse JB, Hogue IB, Feric M, Thiberge SY, Sodeik B, Brangwynne CP, Enquist LW.** 2015. Remodeling nuclear architecture allows efficient transport of herpesvirus capsids by diffusion. Proc Natl Acad Sci U S A **112:**E5725–E5733. http://dx.doi.org/10.1073/pnas.1513876112.

46. **Ben-Porat T, Shimono H, Kaplan AS.** 1970. Synthesis of proteins in cells infected with herpesvirus. IV. Analysis of the proteins in viral particles isolated from the cytoplasm and the nucleus. Virology **41:**256–264.

47. **Addison C, Rixon FJ, Preston VG.** 1990. Herpes simplex virus type 1 UL28 gene product is important for the formation of mature capsids. J Gen Virol **71:**2377–2384. http://dx.doi.org/10.1099/0022-1317-71-10-2377.

48. **al-Kobaisi MF, Rixon FJ, McDougall I, Preston VG.** 1991. The herpes simplex virus UL33 gene product is required for the assembly of full capsids. Virology **180:**380–388. http://dx.doi.org/10.1016/0042-6822(91)90043-B.

49. **Poon AP, Roizman B.** 1993. Characterization of a temperature-sensitive mutant of the UL15 open reading frame of herpes simplex virus 1. J Virol **67:**4497–4503.

50. **Tengelsen LA, Pederson NE, Shaver PR, Wathen MW, Homa FL.** 1993. Herpes simplex virus type 1 DNA cleavage and encapsidation require the product of the UL28 gene: isolation and characterization of two UL28 deletion mutants. J Virol **67:**3470–3480.

51. **Fuchs W, Klupp BG, Granzow H, Leege T, Mettenleiter TC.** 2009. Characterization of pseudorabies virus (PrV) cleavage-encapsidation proteins and functional complementation of PrV pUL32 by the homologous protein of herpes simplex virus type 1. J Virol **83:**3930–3943. http://dx.doi.org/10.1128/JVI.02636-08.

52. **Newcomb WW, Homa FL, Thomsen DR, Ye Z, Brown JC.** 1994. Cell-free assembly of the herpes simplex virus capsid. J Virol **68:**6059–6063.

53. **Thomsen DR, Roof LL, Homa FL.** 1994. Assembly of herpes simplex virus (HSV) intermediate capsids in insect cells infected with recombinant baculoviruses expressing HSV capsid proteins. J Virol **68:**2442–2457.

54. **Kennard J, Rixon FJ, McDougall IM, Tatman JD, Preston VG.** 1995. The 25 amino acid residues at the carboxy terminus of the herpes simplex virus type 1 UL26.5 protein are required for the formation of the capsid shell around the scaffold. J Gen Virol **76:**1611–1621. http://dx.doi.org/10.1099/0022-1317-76-7-1611.

55. **Trus BL, Booy FP, Newcomb WW, Brown JC, Homa FL, Thomsen DR, Steven AC.** 1996. The herpes simplex virus procapsid: structure, conformational changes upon maturation, and roles of the triplex proteins VP19c and VP23 in assembly. J Mol Biol **263:**447–462. http://dx.doi.org/10.1016/S0022-2836(96)80018-0.

56. **Zhou ZH, He J, Jakana J, Tatman JD, Rixon FJ, Chiu W.** 1995. Assembly of VP26 in herpes simplex virus-1 inferred from structures of wild-type and recombinant capsids. Nat Struct Biol **2:**1026–1030. http://dx.doi.org/10.1038/nsb1195-1026.

57. **Trus BL, Homa FL, Booy FP, Newcomb WW, Thomsen DR, Cheng N, Brown JC, Steven AC.** 1995. Herpes simplex virus capsids assembled in insect cells infected with recombinant baculoviruses: structural authenticity and localization of VP26. J Virol **69:**7362–7366.

58. **Trus BL, Newcomb WW, Cheng N, Cardone G, Marekov L, Homa FL, Brown JC, Steven AC.** 2007. Allosteric signaling and a nuclear exit strategy: binding of UL25/UL17 heterodimers to DNA-filled HSV-1 capsids. Mol Cell **26:**479–489. http://dx.doi.org/10.1016/j.molcel.2007.04.010.

59. **Zhou ZH, Dougherty M, Jakana J, He J, Rixon FJ, Chiu W.** 2000. Seeing the herpesvirus capsid at 8.5 A. Science **288:**877–880. http://dx.doi.org/10.1126/science.288.5467.877.

60. **Toropova K, Huffman JB, Homa FL, Conway JF.** 2011. The herpes simplex virus 1 UL17 protein is the second constituent of the capsid vertex-specific component required for DNA packaging and retention. J Virol **85:**7513–7522. http://dx.doi.org/10.1128/JVI.00837-11.

61. **Aksyuk AA, Newcomb WW, Cheng N, Winkler DC, Fontana J, Heymann JB, Steven AC.** 2015. Subassemblies and asymmetry in assembly of herpes simplex virus procapsid. mBio **6:**e01525-01515. http://dx.doi.org/10.1128/mBio.01525-15.

62. **Baker TS, Newcomb WW, Booy FP, Brown JC, Steven AC.** 1990. Three-dimensional structures of maturable and abortive capsids of equine herpesvirus 1 from cryoelectron microscopy. J Virol **64:**563–573.

63. **Perdue ML, Cohen JC, Randall CC, O'Callaghan DJ.** 1976. Biochemical studies of the maturation of herpesvirus nucleocapsid species. Virology **74:**194–208. http://dx.doi.org/10.1016/0042-6822(76)90141-0.

64. **Desai P, Person S.** 1998. Incorporation of the green fluorescent protein into the herpes simplex virus type 1 capsid. J Virol **72:**7563–7568.

65. **Nagel CH, Dohner K, Binz A, Bauerfeind R, Sodeik B.** 2012. Improper tagging of the non-essential small capsid protein VP26 impairs nuclear capsid egress of herpes simplex virus. PLoS One **7:**e44177. http://dx.doi.org/10.1371/journal.pone.0044177.

66. **Krautwald M, Maresch C, Klupp BG, Fuchs W, Mettenleiter TC.** 2008. Deletion or green fluorescent protein tagging of the pUL35 capsid component of pseudorabies virus impairs virus replication in cell culture and neuroinvasion in mice. J Gen Virol **89:**1346–1351. http://dx.doi.org/10.1099/vir.0.83652-0.

67. **Booy FP, Trus BL, Newcomb WW, Brown JC, Conway JF, Steven AC.** 1994. Finding a needle in a haystack: detection of a small protein (the 12-kDa VP26) in a large complex (the 200-MDa capsid of herpes simplex virus). Proc Natl Acad Sci U S A **91:**5652–5656. http://dx.doi.org/10.1073/pnas.91.12.5652.

Supplemental Table 1. Mass spectrometry results from wild-type PRV VP24 29 kD band.

Protein	Virus Gene	Score	Coverage	# Proteins	# Unique Peptides	# Peptides	# PSMs	# AAs	MW [kDa]	calc. pI
pUL26 (includes the 25 kD VP24 product)	UL26	1424.19	44.78	1	21	21	505	527	54.9	7.66
VP5 (major capsid protein)	UL19	959.78	62.41	1	63	63	370	1330	145.8	6.49
VP19c (capsid triplex protein)	UL38	250.66	55.98	1	16	16	91	368	39.9	8.24
Trypsin		216.80	58.87	3	10	10	79	231	24.4	7.18
Mitochondrial Rho GTPase		192.66	24.92	1	13	13	63	618	71.2	6.37
VP23 (capsid triplex protein)	UL18	133.61	52.03	1	14	14	75	296	31.7	8.31
pUL25	UL25	117.98	38.95	1	16	16	45	534	57.3	6.86
pUL17	UL17	113.26	38.02	1	19	19	47	597	64.1	8.81
VP26 (capsid hexon trip protein)	UL35	106.82	79.61	1	6	6	40	103	11.5	9.06
Thymidine kinase	UL23	54.47	38.75	1	9	9	21	320	34.9	7.12
pUS2	US2	41.93	29.69	1	6	6	14	256	27.7	10.77
pUL34	UL34	41.71	43.08	1	7	7	19	260	27.9	9.26
dUTPase	UL50	39.39	48.88	1	12	12	19	268	28.6	8.88
Keratin 1		35.59	11.61	2	7	7	15	629	65.2	8.15
Uncharacterized protein		35.31	13.24	2	4	4	10	423	46.3	6.92
ICP8	UL29	27.21	7.14	1	7	7	13	1177	125.0	6.79
pUL31	UL31	25.11	24.35	1	5	5	11	271	30.4	8.78
Uncharacterized protein		24.80	9.08	1	6	6	12	573	58.0	4.98
Uncharacterized protein		24.38	6.12	1	4	5	11	605	63.4	7.74
Heat shock protein beta-1		22.83	27.05	1	4	4	9	207	22.9	6.70
Vimentin		22.02	12.02	1	4	5	10	466	53.6	5.12
Heterogeneous nuclear ribonucleoprotein A2/B1		20.97	12.90	1	4	4	9	341	36.0	8.65
Capsid portal protein	UL6	20.38	7.31	1	5	5	9	643	70.2	7.55
VP1/2	UL36	16.77	1.55	1	4	4	7	3095	325.5	6.24
VP11/12	UL46	14.56	6.64	1	3	3	4	693	75.5	6.70
60S ribosomal protein L10		13.90	16.82	1	3	3	6	214	24.6	10.14
Uncharacterized protein		13.36	15.71	1	2	2	5	210	23.6	6.38
Ubiquitin B		9.86	41.63	5	2	2	3	209	23.5	6.62
Helixase subunit	UL5	8.53	3.24	1	2	2	3	833	92.0	6.47
pUL16	UL16	7.96	8.23	1	2	2	3	328	34.8	8.15
Beta actin		7.60	12.34	6	3	3	5	235	26.1	5.16
DNA polymerase/replicase	UL42	7.20	7.03	1	2	2	5	384	40.3	6.84
Uncharacterized protein		5.98	10.94	1	2	2	2	192	21.8	9.95
Uncharacterized protein		5.17	15.60	3	2	2	3	109	12.7	8.03
Ran		3.70	20.39	2	2	2	3	103	12.1	9.39

Supplemental Table 2. Mass spectrometry results from PRV-GS5298 GFP-VP24 50 kD band.

Protein	Virus Gene	Score	Coverage	# Proteins	# Unique Peptides	# Peptides	# PSMs	# AAs	MW [kDa]	calc. pI
VP5	UL19	960.66	60.68	1	65	65	403	1330	145.8	6.49
GFP		514.47	55.46	1	14	14	193	238	26.9	6.06
pUL26 (includes the 25 kD VP24 product)	UL26	396.42	35.86	1	17	17	142	527	54.9	7.66
Vimentin		321.69	74.89	1	42	45	137	466	53.6	5.12
Uncharacterized protein		227.84	61.35	1	14	16	77	414	45.6	5.50
VP19c (capsid triplex protein)	UL38	200.68	52.45	1	16	16	77	368	39.9	8.24
pUL32	UL32	160.40	42.98	1	18	18	74	470	51.5	6.99
Trypsin		158.89	43.29	3	7	7	69	231	24.4	7.18
Protein kinase	US3	148.27	63.69	1	16	16	64	336	37.0	5.01
pUL17	UL17	139.26	43.38	1	21	21	58	597	64.1	8.81
ICP8	UL29	129.60	35.51	1	28	28	52	1177	125.0	6.79
pUL25	UL25	122.34	42.88	1	16	16	49	534	57.3	6.86
VP16	UL48	118.08	41.89	1	14	14	45	413	45.1	5.73
Capsid portal protein	UL6	84.41	32.97	1	17	17	33	643	70.2	7.55
Uncharacterized protein		83.15	31.63	2	6	9	32	449	49.2	6.30
RR1	UL39	64.36	36.08	1	21	21	34	790	86.4	7.81
Ubiquitin B		62.29	61.57	5	5	5	30	229	25.7	7.43
pUL37	UL37	61.74	22.74	1	14	14	26	919	98.1	5.41
Tubulin alpha-1B chai		46.81	33.04	2	11	11	20	451	50.1	5.06
VP13/14	UL47	39.44	15.16	1	8	8	13	739	79.4	5.06
Alk nuclease	UL12	39.16	22.57	1	11	11	21	483	51.2	6.47
Uncharacterized protein		36.97	30.55	2	8	8	16	275	30.3	8.51
Keratin 1		36.81	6.84	2	5	5	16	629	65.2	8.15
Actin, cytoplasmic 1		34.12	21.33	2	5	5	13	375	41.8	5.48
Uncharacterized protein		34.01	16.70	1	6	6	11	467	52.3	7.21
pUL21	UL21	31.14	15.49	1	5	5	10	523	55.0	6.13
Uncharacterized protein		30.47	23.52	1	10	12	23	489	54.4	5.82
VP1/2	UL36	28.88	3.33	1	6	6	9	3095	325.5	6.24
Uncharacterized protein		26.78	23.86	2	6	6	12	306	33.3	9.82
Uncharacterized protein		25.67	7.77	1	5	6	13	605	63.4	7.74
gC	UL44	24.92	17.54	1	5	5	10	479	51.2	6.80
ROD1		23.68	14.34	1	6	6	10	523	56.5	9.20
VP23 (capsid triplex protein)	UL18	23.01	19.26	1	5	5	11	296	31.7	8.31
Uncharacterized protein		22.76	8.20	1	5	5	11	573	58.0	4.98
DNA polymerase/replicase	UL42	21.10	17.19	1	5	5	11	384	40.3	6.84
Uncharacterized protein		17.29	14.04	1	4	4	7	406	43.3	8.56
Helicase/primase	UL8	15.82	6.74	1	3	3	6	682	71.1	7.01
VP11/12	UL46	15.63	7.65	1	4	4	6	693	75.5	6.70
Uncharacterized protein		15.19	10.09	1	3	3	5	426	47.9	11.03
VP26 (hexon tip protein)	UL35	15.03	50.49	1	4	4	6	103	11.5	9.06
Helicase subunit	UL5	14.10	6.48	1	4	4	7	833	92.0	6.47
Terminase subunit	UL15	14.01	6.35	1	4	4	7	740	79.6	8.60
Uncharacterized protein		13.23	11.17	1	4	4	7	412	45.7	6.48
gD	US6	12.95	11.44	1	4	4	7	402	44.5	9.31
Elongation factor 1-alpha		12.94	14.07	1	5	5	6	462	50.1	9.01
Glycogen synthase kinase 3 alpha		11.42	12.42	2	4	4	6	483	51.0	8.85
Mitochondrial Rho GTPase		11.38	4.21	1	2	2	4	618	71.2	6.37
Uncharacterized protein		11.33	9.05	1	4	4	6	475	54.3	6.42
Uncharacterized protein		10.41	5.56	1	2	2	4	468	50.4	6.39
Uncharacterized protein		10.06	8.00	1	2	2	4	375	40.7	8.54
Enolase		9.83	7.91	1	2	2	4	354	38.1	8.88
Uncharacterized protein		9.18	9.07	1	3	3	5	397	44.8	7.08
ICP22	US1	8.85	9.17	1	2	2	3	349	37.9	3.94
Uncharacterized protein		8.81	5.26	1	2	2	4	456	50.9	9.14
RNA binding protein fox-1 homolog		8.17	13.01	1	3	3	3	392	41.6	9.09
dUTPase	UL50	7.72	7.46	1	2	2	4	268	28.6	8.88
pUL31	UL31	7.60	16.24	1	3	3	4	271	30.4	8.78
Annexin		7.03	7.34	2	3	3	3	463	49.8	7.05
Uncharacterized protein		6.87	5.99	4	2	2	4	401	45.5	6.23
pUL16	UL16	6.75	9.15	1	2	2	3	328	34.8	8.15
Uncharacterized protein		6.36	3.48	3	2	2	3	661	73.1	7.18
Uncharacterized protein		6.00	5.19	1	2	2	4	520	53.4	9.45
Origin-binding protein	UL9	4.59	4.05	1	2	2	3	840	90.1	8.32
gI	US7	4.34	8.47	1	2	2	4	366	38.7	9.10
Uncharacterized protein		1.90	6.10	1	2	2	2	492	49.9	8.97
eIF3E		0.00	4.26	1	2	2	2	446	52.4	6.40
Uncharacterized protein		0.00	7.27	1	2	2	3	399	42.9	8.91